Open Archive Toulouse Archive Ouverte (OATAO)

Surface Characterization and Properties of Ordered Arrays of CeO₂ Nanoparticles Embedded in Thin Layers of SiO₂

J. Y. Chane-Ching,*,† M. Airiau,† A. Sahibed-dine,‡,§ M. Daturi,§ E. Brendlé,∥
F. Ozil,∥ A. Thorel,⊥ and A. Corma#

Rhodia Recherches, 52 rue de la Haie Coq, 93308 Aubervilliers, France, Faculté des Sciences, Université Chouaib Doukkali, B.P. 20, El Jadida, Morocco, Laboratoire Catalyse et Spectrochimie, ENSICAEN, 6 Bld Maréchal Juin, 14050 Caen Cedex, France, IGCLab, Carreau Rodolphe, Route de Guebwiller, 68480 Pulversheim, France, ENSMP, Centre des Materiaux, BP 87, 91003-Evry, France, and Instituto de Tecnologia Quimica, UPV-CSIC, Avd de Los Naranjos, 46022 Valencia, Spain

We demonstrated the surface composite character down to the nanometer scale of SiO_2-CeO_2 composite high surface area materials, prepared using 5 nm colloidal CeO_2 nanoparticle building blocks. These materials are made of a homogeneous distribution of CeO_2 nanoparticles in thin layers of SiO_2, arranged in a hexagonal symmetry as shown by small-angle X-ray scattering and transmission electron microscopy. Since the preparation route of these composite materials was selected in order to produce SiO_2 wall thickness in the range of the CeO_2 nanoparticle diameter, these materials display surface nanorugosity as shown by inverse chromatography. Accessibility through the porous volume to the functional CeO_2 nanoparticle surfaces was evidenced through an organic acid chemisorption technique allowing quantitative determination of CeO_2 surface ratio. This surface composite nanostructure down to the nanometer scale does not affect the fundamental properties of the functional CeO_2 nanodomains, such as their oxygen storage capacity, but modifies the acid-base properties of the CeO_2 surface nanodomains as evidenced by Fourier transform IR technique. These arrays of accessible CeO_2 nanoparticles displaying high surface area and high thermal stability, along with the possibility of tuning their acid base properties, will exhibit potentialities for catalysis, sensors, etc.

Introduction

Optical,[1] electrical,[2] magnetic,[3] and catalytic[4] properties of materials can be tuned by varying their sizes in the nanometer size regime. Considerable efforts have been devoted to manipulate nanosize objects to exploit their beneficial properties.[5-7] Ordered nano-object assemblies can enhance some of their properties and widen their range of applications.[8-11] For instance, controlled structuring through the control over interparticle separation could provide a means for controlling both quantum and classical coupling interactions.[12] Strong magnets with excellent magnetic properties were fabricated through the self-assembly of mixtures of magnetic nanoparticles.[9] The effort to understand the physics of ordered arrays of nano-objects has been paralleled by attempts to construct arrays with controlled composition and architecture.[10,13-15]

These arrays are usually induced by slow evaporation of the carrier solvent after ultrasonic agitation of the solvent dispersions.[9,10] Ligand exchange of the long chain surface capping group allowed the interparticle distance to be adjusted. Self-assembly alone however produces simple close packed arrays of colloidal particles. To generate more complex crystal lattices, one should create periodic potentials for self-assembly of colloidal spheres.[16] Recently emulsion droplets were used to template self-assembly of colloidal spheres of 844 nm polystyrene (PS) spheres.[17] During the evaporation of the toluene droplets, the PS spheres strongly bound to the toluene droplets packed by capillary forces to form colloidal assembly with a sequence of symmetric patterns. However there are relatively few methods to control the fabrication and arrangement of nanoparticles in three-dimensional (3D) arrays which display high surface area and physical integrity under attrition conditions and sustain high-temperature regimes. A need exists for producing arrays of individual nanoparticles displaying mechanical and high-temperature stability, useful for a variety of applications such as sorption, catalysis, etc.

Our approach involves the use of nanoparticle building blocks and their self-assembly using a mineral binder.

† Rhodia Recherches.
‡ Université Chouaib Doukkali.
§ Laboratoire de Catalyze et de Spectrochimie, ISMRA.
∥ IGCLab, Carreau Rodolphe.
⊥ ENSMP, Centre des Materiaux.
Instituto de Tecnologia Quimica, UPV-CSIC.
(1) Brus, E. L. *Chem. Phys.* **1984**, *80*, 4403.
(2) Kastner, M. A. *Phys. Today* **1993**, *46*, 1, 24.
(3) Bean, C. P.; Livingston, J. D. *J. Appl. Phys.* **1959**, *30*, 1208.
(4) Lewis, L. N. *Chem. Rev.* **1993**, *93*, 2693.
(5) Colvin, V. L.; Schlamp, M. C.; Alivisatos, A. P. *Nature* **1994**, *370*, 354.
(6) Cui, Y.; Lieber, C. M. *Science* **2001**, *291*, 851.
(7) Heiz, U.; Bullock, E. L. *J. Mater. Chem.* **2004**, *14*, 564.
(8) Sellmyer, D. J. *Nature* **2002**, *420*, 374.
(9) Zeng, H.; Li, J.; Liu, J. P.; Wang, Z. L.; Sun, S. *Nature* **2002**, *420*, 395.
(10) Pileni, M. P. *J. Phys. Chem. B* **2001**, *105*, 3358.
(11) Motte, L.; Billoudet, F.; Pileni, M. P. *J. Phys. Chem.* **1995**, *99*, 16425.
(12) Collier, C. P.; Saykally, R. J.; Shiang, J. J.; Henrichs, S. E.; Heath, J. R. *Science* **1997**, *277*, 1978.

(13) Martin, B. R.; Dermody, D. J.; Reiss, B. D.; Fang, M.; Lyon, A.; Natan, M. J.; Mallouk, T. E. *Adv. Mater.* **1999**, *11*, 12, 1021.
(14) Fan, F.; Stebe, K. J. *Langmuir* **2004**, *20*, 3062.
(15) Teng, X.; Yang, H. *J. Mater. Chem.* **2004**, *14*, 774.
(16) Wang, D.; Mohwald, H. *J. Mater. Chem.* **2004**, *14*, 459.
(17) Manoharan, V. N.; Elsesser, M. T.; Pine, D. J. *Science* **2003**, *301*, 483.

Since mesoporous SiO_2 material was largely developed,[18] a co-templating method involving both the precipitation of silica into ordered thin layers in the presence of CeO_2 nanoparticles as functional building blocks is proposed. In this approach, the challenge is to minimize the coverage of the CeO_2 functional nanoparticle by the silica binder allowing significant accessibility to the functional nanoparticle building blocks. The use of CeO_2 nanoparticle building blocks, monodispersed in size (5 nm diameter) offers the advantage to perfectly control the composite structure of the surface down to the nanometer scale.

In this paper, a variety of techniques was used to determine the surface structure down to the nanometer scale of our high surface area materials prepared using the co-self-assembling route. We will show that the resulting ordered arrays of CeO_2 nanoparticles, embedded in thin layers of SiO_2 binder, display an oxygen storage capacity, a functional CeO_2 property,[19] accompanied by some modification of surface acid−base properties differing from those of a pure CeO_2 material. This opens up the possibility of tuning some of the properties of the nanoparticles arrays achieved through an appropriate choice of the mineral binder while preserving the intrinsic property of the functional nanoparticles.

Methods, Materials, and Experimental Procedures

Synthesis and Characteristics of Nanostructured Materials. SiO_2−CeO_2 nanostructured materials with different molar fractions of CeO_2, $C_{CeO_2} = 0.2$ and $C_{CeO_2} = 0.5$ (denoted $Si_{0.8}$−$Ce_{0.2}$ and $Si_{0.5}$−$Ce_{0.5}$, respectively), were prepared using 5 nm diameter CeO_2 nanoparticle building blocks through a co-self-assembly process on a liquid crystal phase template based on an amphiphilic copolymer $HO(CH_2CH_2O)_{20}(CHCH_3CH_2O)_{70}$-$(CH_2CH_2O)_{20}OH$ (designated EO_{20}−PO_{70}−EO_{20} Pluronics P123, BASF). In a typical synthesis (sample $Si_{0.5}$−$Ce_{0.5}$), 10 g of Pluronics P123 was dissolved in 330 cm³ of water and 37.6 cm³ of 2 M HCl, and 25.0 cm³ of a 2 M CeO_2 colloidal dispersion was poured into this solution. Then 10.4 g of tetraethyl orthosilicate (TEOS) was added in one hour at room temperature into the dispersion. The resulting dispersion was first aged at 318 K for 16 h and then aged overnight at 353 K. The solid product was washed and dried, and the copolymer template was removed by calcination at 773 K. As a reference sample, pure SiO_2 nanostructured material was prepared using the same recipe, but without the incorporation of CeO_2 nanoparticles, following a classical procedure.[18] Pure CeO_2 nanostructured material was also synthesized using identical spherical CeO_2 nanoparticles building blocks, through a self-assembly process on a liquid crystal phase using a method described elsewhere.[20] The pure SiO_2 and pure CeO_2 nanostructured materials were calcined at 773 K. A physical mixture composed of pure CeO_2 and pure SiO_2 nanostructured materials was also prepared at a CeO_2 molar ratio of 0.26 (sample denoted $Si_{0.74} + Ce_{0.26}$).

SAXS and Nitrogen Adsorption−Desorption Characterization. The textural characteristics of the mixed oxides were obtained from nitrogen adsorption−desorption isotherms and from small-angle X-ray scattering (SAXS) experiments. The nitrogen adsorption and desorption isotherms were determined at 77 K using a Micromeritics ASAP 2000 system with previous overnight drying of samples under vacuum at 20 °C. The pore size distribution was obtained from the BJH (Barret−Joyner−Halenda) analysis of the desorption branch of the isotherms. SAXS data were collected using the 2 m pinhole instrument fitted with a two-dimensional gas-filled detector operating at a

wavelength of 1.54 Å (Cu Kα radiation) at the Centre d'Etudes de Saclay, France. This instrument is fully described in ref 21.

Electron Microscopy. (A) Electron Microscopy. The high-resolution transmission electron microscopy (HRTEM) investigation was performed with a Tecnai F20/FEG/ST, a 200 kV microscope equipped with a field emission electron gun (FEG), and a super twin objective lens of low spherical and chromatic aberrations (Cs = Cc = 1.2 nm). Point to point resolution is 0.17 nm in high-resolution scanning transmission electron microscopy (HRSTEM) and 0.24 nm in HRTEM, although the high coherency of the beam currently allows imaging distances down to 0.15 nm.

(B) Analytical Equipment. Analytical investigations of the distribution of chemical elements were carried out using an energy Si−Li energy-dispersive X-ray emission spectrometer (EDS) with energy resolution about 1.35 eV. The detector is equipped with a Super Thin Window (SUTW), therefore, light elements down to boron can be detected and quantified. The spatial resolution at which EDS analyses can be carried out is essentially related to the probe size: optimum EDS operating conditions for the present analyses were obtained with a probe size of about 1 nm. The EDS investigations have been coupled to STEM−high-angular annular dark field (HAADF) imaging in order to get a better insight into the repartition of the CeO_2 nanoparticles embedded in SiO_2 thin layers. Note that the HAADF image contrast is approximately the reverse of a conventional TEM bright field micrograph, with pores displayed in black color, low Z atoms in gray, and high Z atoms in white.

(C) Sample Preparation. TEM samples were prepared in cross section after impregnation of the powder in an organic resin. Ultrathin films of 10−30 nm were prepared using an ultramicrotome.

Surface Characteristics Determined by Inverse Gas Chromatography (IGC). IGC is currently applied for the characterization of powders and allows evaluation of surface properties in terms of surface interaction potential and surface nanomorphology.[22,23] In an IGC experiment, chosen probes are injected in a column containing the powder of interest. When determining the time the chosen probe spends in the column (retention time), compared to the corresponding time of a noninteractive or poorly interactive probe, it becomes possible to appreciate the affinity of the support for the probe. When selecting for example alkane probes that are only capable of London or dispersive types of interactions, one may evaluate the dispersive interaction potential or dispersive component of the surface energy of the solid. Choosing probes of given morphologies, but possessing the same interaction potential (London), will lead to information on the solid surface accessibility or on its surface nanomorphology. By injecting very small quantities of probes, one may consider that the adsorbed probe molecules are sufficiently separated so as to become unable to exchange lateral interaction between them: hence their retention time reflects only the probe−solid surface interaction capacity. This type of IGC is called IGC at infinite dilution conditions (IGC-ID).

(A) Preparation of IGC Columns and IGC Measurements. IGC measurements were performed, using commercial equipment (FISONS HRGC Mega 2 series), fitted with a flame ionization detector. The length of the IGC columns was 20 cm and the internal diameter about 2 mm. Before analysis, the oxide surfaces, placed inside the GC columns, were outgassed by heating at 473 K, under a helium flow. Due to the interactivity differences between the various oxide samples, the IGC-ID analysis temperature was adapted to each of them. Chromatograms were recorded at 383 K on SiO_2 and SiO_2−CeO_2 composites and at 413 K on pure CeO_2 material and sample prepared from the physical mixture ($Si_{0.74} + Ce_{0.26}$ sample). The carrier gas (He) flow rate was 20 cm³ min⁻¹.

(B) Dispersive or Nonspecific Component of the Surface Energy. The dispersive component of the surface energy is commonly determined using the Dorris and Gray approach,[24] i.e., by injecting small amounts of n-alkane probes (capable of sole dispersive interactions) in the column filled with the solid

(18) Zhao, D.; Huo, Q.; Feng, J.; Chmelka, B.; Stucky, G. *J. Am. Chem. Soc.* **1998**, *120*, 6024.

(19) Shelef, M.; Graham, G. W.; Gabe, R. Mc. Catalysis by Ceria and Related Materials; Trovarelli, A. Ed.; Imperial College Press: London, 2001.

(20) Corma, A. C.; Atienzar, P.; Garcia, H.; Chane-Ching, J. Y. *Nat. Mater.* **2004**, *3*, 394.

(21) Zemb, T.; Taché O.; Né, F.; Spalla O. *Rev Sci. Instrum.* **2003**, *74*, *4*, 2456.

(22) Brendle, E.; Papirer, E. *J. Colloid Interface Sci.* **1997**, *194*, 207.

(23) Brendle, E.; Papirer, E. *J. Colloid Interface Sci.* **1997**, *194*, 217.

(24) Dorris, G. M.; Gray, D. G. *J. Colloid Interface Sci.* **1979**, *71*, 97.
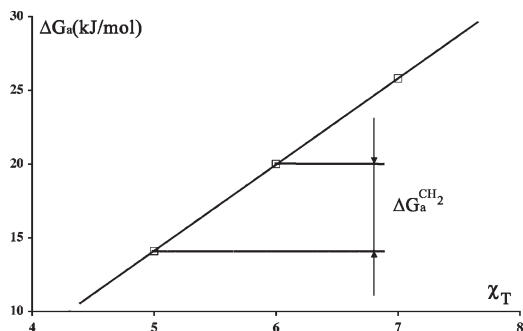
Figure 1. Example of determination of $\Delta G_a^{CH_2}$ on CeO_2 sample, at 413 K.

of interest. The variation of free energy of adsorption of the probe ΔG_a is easily determined since it is directly related to the retention time or retention volume (volume of carrier gas required to push the probe through the column).

The dispersive component of the surface energy (γ_s^d) may be calculated according to the Dorris and Gray relation[1]

$$\gamma_s^{\ d} = \frac{(\Delta G_a^{\ CH_2})^2}{4N^2 a_{CH_2}^{\ 2} \gamma_{CH_2}} \tag{1}$$

where N is Avogadro's number, a_{CH_2} is the area covered by one adsorbed methylene group (0.06 nm^2). γ_{CH_2} is the surface energy of a solid entirely made of methylene groups (i.e., polyethylene). $\Delta G_a^{CH_2}$ is the variation of adsorption free energy of a methylene group. It is given by the slope of the straight line relating the free adsorption energies to the number of carbon atoms of the injected n-alkanes as shown on Figure 1.

The units on the abscissa axis are either the number of C atoms (n_C) of the injected alkane or the topology index (χ_T) that happens to equal to n_C for alkane probes.

(C) IGC-ID Measurements of the Nanomorphology Index. The intensity of interaction of a solid with a solute is governed not only by the theoretical interaction potential but also by the accessibility of the two partners at the molecular layer. IGC-ID is capable of detecting such surface roughness at the molecular level. This is achieved by comparing the behaviors of bulky, branched (or cyclic) hydrocarbons with the ones of flexible n-alkanes. When bulkiness hinders branched or cyclic isomers from entering the structure in which linear alkanes readily adsorb, much lower retention times are observed. Now, when comparing adsorption behaviors of linear and nonlinear alkanes, it is necessary to consider the fact that the molecular structure introduces also a nonnegligible variation of the molecular polarizability that cannot be ignored. Brendlé and Papirer[22,23] defined an adequate (χ_T) topology index, derived from Wiener's molecular topology indexes,[25] in order to take into account both parameters, bulkiness and polarizability, of the molecular probe. Experimentally, size exclusion effects lead to a decrease of retention volumes (or the free energy of adsorption).

The morphology index (IM) is given by the ratio of the retention volume of a branched alkane molecule $V_G(M)$ and $V_G(C)$ the retention volume of a virtual n-alkane having the same topology index. This method is well documented in the literature[22]

$$IM_{(branched\_probes)} = \frac{V_G(M)}{V_G(C)} \tag{2}$$

One may also start from the free adsorption energy

$$IM_{(branched\_probes)} = \exp \frac{\Delta G_a(M)}{\Delta G_a(C)} \tag{3}$$

A value of 1 or close to 1 indicates that both branched and n-alkanes have equivalent accessibility to the surface. In other

terms, we may conclude that the surface is flat at the molecular level. If IM is below 1, the solid's surface exhibits rugosity.

Chemical Determination of the Number of Accessible Surface Groups. The evaluation of the number of accessible surface groups on the different nanostructured materials was made using two reactive organic acids differing by their bulkiness: propionic acid and pivalic acid. Those acids were selected regarding their strong complexing ability towards the Ce^{4+} cation.[26] Moreover, propionic acid scarcely chemisorbs on pyrogenic silica.[27] Its irreversible fixation on the present composite materials may therefore be mainly attributed to the existence of Ce surface groups. The percentage (τ) of irreversibly adsorbed acid was determined by elemental analysis of C, using a LECO CS 444 equipped with a IR detection of CO_2 evolved from the complete oxidation of C. From the percentage of fixed carbon, the graft density (n), expressed as graft/nm^2, was computed according to

$$n = \frac{6023\tau}{12n_C S_m} \tag{4}$$

where n_c is the number of carbon atoms contained in the acid molecule and S_m is the specific surface area determined from nitrogen adsorption isotherms, expressed in m^2 g^{-1}.

In practice, the carboxylic acid grafting was made either in the chromatographic column with propionic acid (in situ technique) or in a desiccator with pivalic acid. Successive injections of 10 μL of pure propionic acid (Aldrich 40,290-7, 99.5+%) were introduced at a temperature of 383 K and under a carrier gas flow of 20 cm^3 min^{-1} until reproducible chromatograms were obtained. Water vapor was then injected in order to hydrolyze the nonstable derivative possibly formed between propionic acid and the surface silanol groups of the silica component of the composite material. Finally, the surface cleaning was followed by a thermal treatment at 473 K for 2 h.

Pivalic acid (Acros Organics 75-98-9 99%) treatment was performed by placing first the composite material in a closed reactor containing solid pivalic acid. Thereafter, the reactor was heated, in an oven, at 383 K during 24 h. Finally, the treated material was submitted to a solvent extraction (ethyl ether) in order to eliminate from the surface all reversibly or physisorbed acid. Additional heating at 333 K allowed removal of the residual solvent.

Determination of the Oxygen Storage Capacity and Acid−Base Properties Using FTIR. Before FTIR examination, the powders were pressed into self-supported wafers of about 10 mg cm^{-2} and introduced in a quartz cell, placed in the IR beam. The wafer was then heated under vacuum (1.3×10^{-4} Pa) up to 773 K. Then, oxygen was introduced in the quartz cell until a pressure of 13 kPa after 1 h of contact was reached. The cell was thereafter outgassed, at the same temperature, for one additional hour. IR spectra were recorded with a Nicolet Magna 550 FT-IR spectrometer (resolution 4 cm^{-1}) after quenching the samples to room temperature. Probe molecules were introduced at room temperature on the activated samples, and the cell was again outgassed. The FTIR spectra were treated using the Nicolet OMNIC software.

For the FTIR studies involving a chemical reduction step, samples were exposed to 13 kPa of H_2 at room temperature, then heated for 0.5 h at the reduction temperature, and evacuated at the same reduction temperature under 1.3×10^{-4} Pa for 15 mn. This procedure was repeated twice.

Modification of acid−base surface properties of CeO_2 nanodomains resulting from the nanostructuration were investigated by FTIR using different probes. CO_2 adsorption on CeO_2 surfaces was usually used to investigate their basic properties through the various carbonate species formed.[28] The adsorbed species could be identified by determining the splitting of the bands arising from the degenerated ν_3 vibration centered at around 1415 cm^{-1}: the presence of polydentate or monodentate carbon-

(25) Wiener, H. *J. Phys. Chem.* **1948**, *52*, 425.

(26) Bouchara, A.; Soler-Illia, G.; Chane-Ching, J. Y.; Sanchez, C. *Chem. Commun.* **2002**, *11*, 1234.
(27) Ozil, F. Ph'D Université de Haute Alsace, 26 octobre 1999.
(28) Payen, E.; Grimblot, J.; Lavalley, J. C.; Daturi, M.; Mauge, F. *Handbook of Vibrational Spectroscopy*; Wiley: New York, 2002; Vol. 4.
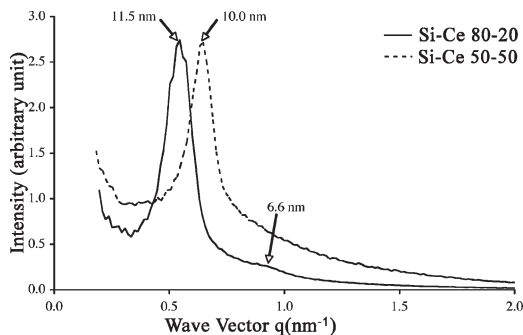
Figure 2. SAXS patterns of $Si_{0.8}Ce_{0.2}$ and $Si_{0.5}Ce_{0.5}$ materials prepared using CeO_2 nanoparticles building blocks and calcined at 773 K. The most distinct hexagonal crystalline pattern was associated with the sample prepared with C_{CeO2} = 0.2.

ates usually produces a split value $\Delta\nu_3 < 150$ cm^{-1}, for bidentate carbonates 150 cm^{-1} $< \Delta\nu_3 < 400$ cm^{-1}, and for bridging carbonates $\Delta\nu_3 > 400$ cm^{-1}. The thermal stability of these species ranged in the following order: monodentates < bidentates < polydentates. In our experiments, after activation of the materials following the previously described conditions, adsorption of CO_2 was performed at 1.3×10^3 Pa in equilibrium conditions. Evacuation at different temperatures was carried out in order to determine the stability of the adsorbed carbonate species.

Results and Discussion

1. An Ordered Array of CeO₂ Nanoparticles Embedded in SiO₂ Thin Layers. SAXS patterns (Figure 2) of the $Si_{0.8}Ce_{0.2}$ material exhibit a peak centered at 115 Å and a less intense peak at 66 Å, indicating a hexagonal structure. In contrast for the $Si_{0.5}Ce_{0.5}$ material, the SAXS pattern displays an unique peak centred at 100 Å suggesting a less ordered material. Nitrogen adsorption−desorption isotherm curves exhibited well-defined steps indicating the existence of uniform mesopores in the range of 4 nm for these two materials.

Mesostructures of the $Si_{0.5}Ce_{0.5}$ material were determined by TEM investigations. In plane view, TEM thin sections of the $Si_{0.8}Ce_{0.2}$ materials prepared by ultramicrotomy showed well-ordered large bright channels with a hexagonal symmetry configuration (Figure 3a). In a side view using a different cross section, the bright areas appear as cylinders having parallel orientation and sandwiched between 5 nm wide dark contrast walls composed of strings of crystalline nanoparticles (Figure 3b). These combined observations suggest that these bright areas consisted of 5 nm wide cylindrical pores arranged in a hexagonal symmetry (Figure 3a). High-resolution observations coupled with a Fourier analysis allow the determination that the walls are made of a homogeneous mixture of highly diffracting 5 nm wide CeO_2 nanoparticles (0.18, 0.25, and 0.27 nm spacing), embedded in a vitreous silica matrix (halo centered at 0.34 nm). The typical spacing of resin macromolecules has also been found (0.5−0.7 nm) since resin was used for the TEM sample impregnation.

Ce, Si, C, and O concentration profiles across alternately bright and dark areas were investigated using EDS coupled STEM−HAADF (Figure 4). Similar evolutions of the Ce and Si concentration profiles were recorded: low Ce and Si concentrations were determined when crossing the pore domains, whereas high concentrations were recorded within the mineral thin layers. The Ce and Si concentration profiles exhibited maximums generally slightly shifted by 1.0 nm, value corresponding to the step between two EDS successive analysis. These Ce concentration maximums were observed for local concentration profiles exhibiting a width of approximately the size of one single CeO_2 nanoparticle. The simultaneous presence

observed for Ce and Si in the thin layers for all the concentration profiles we carried out gives evidence of the intimate and homogeneous distribution of the CeO_2 nanoparticles in the silica thin layers.

From all these observations it can be inferred that the CeO_2 nanoparticles are individualized and homogeneously distributed in the silica thin layers resulting in an ordered array of CeO_2 nanoparticles embedded in thin layers of SiO_2 arranged in a hexagonal symmetry.

Textural characteristics of studied samples are presented in Table 1.

The SAXS and TEM investigations have shown the formation of an ordered array of CeO_2 nanoparticles embedded in silica thin layers possessing a thickness slightly larger than the CeO_2 nanoparticle size. However, at this stage, we do not have any evidence of the surface nanostructure by the CeO_2 nanoparticles. To get a better insight in the surface nanostructure, $Si_{0.8}-Ce_{0.2}$ and $Si_{0.5}-Ce_{0.5}$ materials were investigated by IGC and FTIR techniques.

2. Surface Nanorugosity of the Nanostructured Composites. Adsorption behavior of linear (n-alkanes) and nonlinear alkanes (cyclohexane and 2,2-dimethylbutane) on $Si_{0.5}Ce_{0.5}$ materials are reported in Figure 5. The representative points of the latter probes are clearly below the alkane line demonstrating thus the existence of nanoroughness on the given composite oxide samples.

The morphology index (IM) values of the studied oxides are reported in Table 2.

Mesostructured silica displays a morphological index value of 0.96 when determined with dimethylhexane and 0.98 for cyclooctane. Those values, close to 1, point to the existence of a rather flat surface whatever the branched or cyclic alkane probe used to test the surface morphology. A morphological index value lower than 1, indicating nanorugosity, was determined for the pure CeO_2 materials, consistent with the preparation route of this material involving self-assembly of CeO_2 nanoparticles. Significantly lower IM values are observed for composite ordered arrays of nanoparticles. This surface nanorugosity observed on these materials prepared using nanoparticles building blocks suggests that the CeO_2 nanoparticles building blocks significantly affected the surface morphology.

3. Assessment of the Surface Heterogeneity with Surface Accessibility of the CeO₂ Nanodomains of the SiO₂−CeO₂ Composites. To show a composite aspect of the surface, that is, a surface nanostructure consisting of CeO_2 patch domains resulting from embedded CeO_2 nanoparticle bumps, a description of the chemical nature of the surfaces was performed using, first, a macroscopic surface energy term, the dispersive component of the surface energy γ_s^d, and, second, measuring the acid chemisorption capacity of CeO_2 specific probes.

Surface Interaction Potential. $\Delta G_a^{CH_2}$ and γ_s^d values, determined from IGC-ID experiments on the different studied materials, are reported in Table 3. The dispersive component of the surface energy, γ_s^d, of the SiO_2 mesostructured material is equal to 40 ± 2 mJ m^{-2}. A higher value is observed with nanostructured CeO_2 for which $\gamma_s^d = 230 \pm 9$ mJ m^{-2}. Intermediate values measured on the nanostructured composite materials suggest that the composite materials display CeO_2 and SiO_2 surfaces.

Table 3 relates the surface energy values determined on the sample made of a physical mixture of mesostructured SiO_2 and nanostructured CeO_2 materials. A value of 200 ± 7 mJ m^{-2} was obtained for this sample (sample $Si_{0.74}-Ce_{0.26}$). Although γ_s^d applies to the sole energetic homogeneous materials, those observations show never-
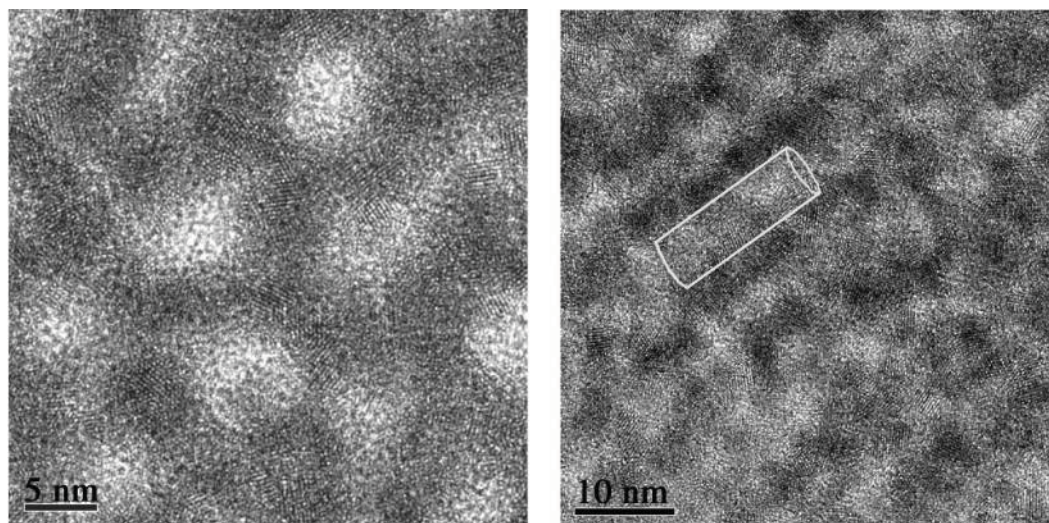
Figure 3. TEM images of $Si_{0.5}-CeO_{0.5}$ material. Scale bar = 5 nm. (a) Cross section showing hexagonally ordered mesoporosity (filled with resin). CeO_2 crystalline planes can be viewed on this high magnification micrograph. (b) Small fragment viewed parallel to cylindrical pores sandwiched between strings of CeO_2 nanoparticles embedded in silica.
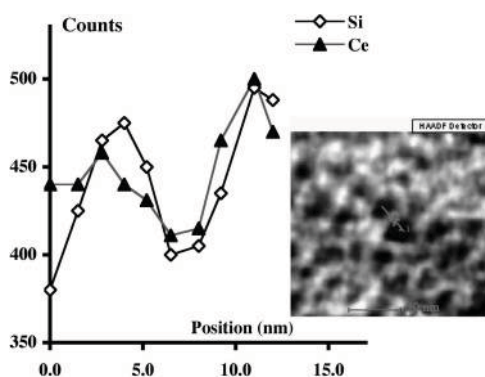

Figure 4. EDS coupled STEM-HAADF investigation of $Si_{0.5}-Ce_{0.5}$ materials. In the HAADF mode, pores appear as dark areas and mineral framework appears as bright areas. Si and Ce concentration profiles crossing alternately bright and dark areas showed similar evolutions of Ce and Si.

Table 1. Structural and Morphological Characteristics of Studied Samples

	$SiO_2{}^a$	$Si_{0.8}-Ce_{0.2}{}^a$	$Si_{0.5}-Ce_{0.5}$	CeO_2
structure	hexagonal	hexagonal	hexagonal	hexagonal
d_{SAXS} (nm)	10.2	11.5	9.8	10.2
V_p (cm^3 g^{-1})	0.81	0.60	0.3	0.3
D_p (nm)	6	4	4	5
e^b (nm)	6	9.5	7.5	7
S^b (m^2/g)	906	663	310	165

^{a} These materials exhibit micropores (D_p < 2 nm). Surface area and porous volume corresponding to the micropores are evaluated to be 440 m^2 g^{-1} and 0.19 cm^3 g^{-1} (SiO_2) and to be 270 m^2 g^{-1} and 0.12 cm^3 g^{-1} ($Si_{0.8}-Ce_{0.2}$), respectively. Wall thickness was determined from d_{SAXS} and pore diameter assuming a hexagonal structure with a cell parameter $a = 2d_{SAXS}/3^{1/2}$. ^{b} e and S represent the wall thickness and the surface area, respectively.

theless completely different behavior for nanostructured SiO_2-CeO_2 composite materials, compared to a physical mixture composed of mesostructured SiO_2 and nanostructured CeO_2 materials.

Determination of the Number of Accessible Ce Surface Sites. As indicated above, the chemical fixation of organic acid constitutes a direct way for the evaluation of the Ce surface reactive groups. Table 4 displays the results in terms of C content of the oxides after reaction and subsequent purification as well as the number of grafts per unit surface area (determined by
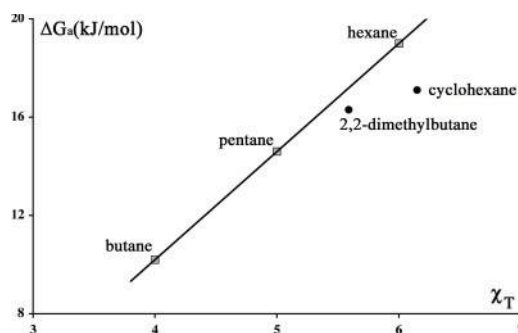

Figure 5. Comparison of the behaviors of linear and branched or cyclic alkanes on $Si_{0.5}Ce_{0.5}$ materials at 383 K.

nitrogen, adsorption).On the reference silica, grafting densities of 0.15 and 0.12 molecule/nm^2 were noted with propionic and pivalic acids, respectively (these values are close to those obtained by Ozil on A130[27]). These values lead to a surface coverage of about 6%. Comparatively, surface coverage ratios of 95 and 87% were determined with propionic and pivalic acids, respectively, on the nanostructured pure CeO_2 reference material. The lower value determined for the pivalic acid problably results from a surface nanorugosity effect combined to a steric hindrance effect. Concerning the SiO_2-CeO_2 nanostructured composites, CeO_2 surface coverage ratios of 13% and 30% were determined on the materials prepared at $C_{CeO_2} = 0.2$ and $C_{CeO_2} = 0.5$, respectively, using propionic acid. These data demonstrated accessibility to the CeO_2 surface and indicated a partial embedding of the CeO_2 nanoparticles in the silica layers arranged in an hexagonal symmetry.

The SiO_2-CeO_2 composite materials consisted of 5 nm CeO_2 nanoparticles homogeneously distributed in the SiO_2 thin textured framework. EDS/TEM investigations suggested that the CeO_2 nanoparticles could emerge from the SiO_2 thin layer and be accessible through the pore or, on the contrary, be totally embedded by the silica thin layers. These CeO_2 nanoparticles, located near the surfaces, produced a surface nanorugosity as evidenced by IGC-ID experiments. The surfaces of these CeO_2 nanoparticles partially embedded in the thin layers of silica are accessible through the porous volume as shown by chemisorption of propionic acid. The surface coverage ratio by the CeO_2 nanodomains was determined to be 30% for

Table 2. Morphology Index (IM) Determined Using Various Probes

	morphology index			
	SiO$_2$	Si$_{0.8}$–Ce$_{0.2}$	Si$_{0.5}$–Ce$_{0.5}$	CeO$_2$
2,2-dimethylhexane	0.96 ± 0.04			
2,2-dimethylbutane		0.67 ± 0.03	0.77 ± 0.02	
cyclohexane		0.42 ± 0.03	0.46 ± 0.01	
cycloheptane				0.50 ± 0.02
cyclooctane	0.98 ± 0.05			

Table 3. Comparison of "Apparent" Dispersive Components of Surface Energy Measured on Mixtures of Silica and Cerium Oxide and on the Composite Oxide Materials
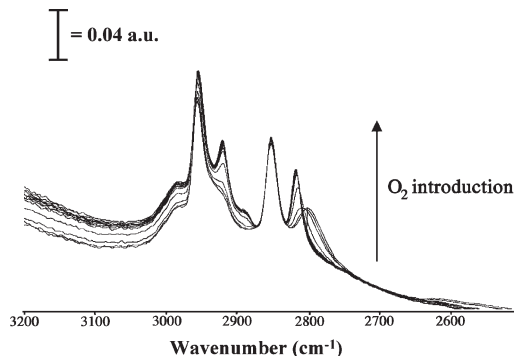
	γ_s^d (mJ/m^2)	$\Delta G_a^{CH_2}$ (kJ/mole)
SiO$_2$	39 ± 2	2.5 ± 0.1
Si$_{0.8}$–Ce$_{0.2}$	108 ± 4	4.1 ± 0.1
Si$_{0.5}$–Ce$_{0.5}$	120 ± 5	4.4 ± 0.4
Si$_{0.74}$ + Ce$_{0.26}$	200 ± 7	5.5 ± 0.2
CeO$_2$	230 ± 9	5.9 ± 0.1

Table 4. Determination of the CeO$_2$ Surface Sites by Chemisorption of Organic Acids

	SiO$_2$	Si$_{0.8}$–Ce$_{0.2}$	Si$_{0.5}$–Ce$_{0.5}$	CeO$_2$
propionic acid (30 Å^2)				
% C	0.81	1.71	1.82	2.67
n (graft/nm^2)	0.15	0.43	0.98	2.71
% cov surface	5	13	30	95
pivalic acid (45 Å^2)				
% C	1.07	1.65	1.05	2.74
n (graft/nm^2)	0.12	0.25	0.34	1.67
% cov surface	6	11	16	87

the Si$_{0.5}$–Ce$_{0.5}$ material. From all these observations, we can conclude that a large proportion of the CeO$_2$ nanoparticles emerges from the SiO$_2$ thin layers resulting in SiO$_2$–CeO$_2$ surfaces displaying a composite structure down to the nanometer scale.

4. Effect of the Composite Nanostructure of the Surface on Some Properties of the SiO$_2$–CeO$_2$ Composite Materials. Oxygen storage capacity (OSC) of CeO$_2$ nanodomains of the SiO$_2$–CeO$_2$ composite materials was investigated in order to evaluate a functional property involving both surface and bulk CeO$_2$. The chemisorption of CH$_3$OH on the CeO$_2$ surface proceeds through a dissociative mode, with breaking off OH bonds, resulting in a Ce^{x+}···OCH$_3$ methoxy formation, with x = +3 or +4.[29,30] Since the ν(OC) vibration frequencies of those methoxy species are depending on the oxidation state of the cerium cation (1107 and 1062 cm^{-1} for linear and bridged Ce^{4+}···OCH$_3$ species, respectively, and ~1083 cm^{-1} for bridged Ce^{3+}···OCH$_3$, whereas linear Ce^{3+}···OCH$_3$ is not observed[31]), this dissociative adsorption of methanol is a valuable method for testing and evaluating the oxidation state of the cerium cation in a CeO$_2$ sample. Moreover, the exposure to oxygen at room temperature produces a reversible Ce^{3+} → Ce^{4+} transformation, with a consequent and progressive decreasing of the signal corresponding to bridged Ce^{3+}···OCH$_3$ and recovering of the band at 1107 cm^{-1}, corresponding to linear species on Ce^{4+}. Thus, by applying FTIR and using the methanol probe, it becomes possible to determine the OSC of the materials through the determination of the amount of oxygen needed to fully reoxidize the samples.[31,32] We determined a value of 270 μmol of O$_2$ per gram of catalyst

(29) Daturi, M.; Binet, C.; Lavalley, J. C.; Galtayries, A.; Sproken, R. *Phys. Chem. Chem. Phys.* **1999**, *1*, 5717.
(30) Daturi, M.; Binet, C.; Lavalley, J. C.; Blanchard, G. *Surf. Interface Anal.* **2000**, *30*, 273.
(31) Binet, C.; Daturi, M. *Catal. Today* **2001**, *70*, 155.
(32) Binet, C.; Daturi, M.; Lavalley, J. C. *Catal. Today* **1999**, *50*, 207.
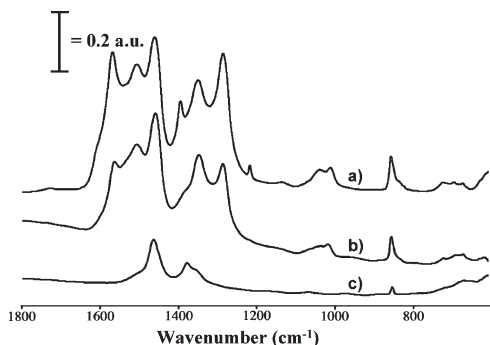
Figure 6. Evolution of the methoxy spectra during the reoxidation of the SiO$_2$–CeO$_2$ sample. Region of the ν(CH$_3$) stretch.

for the OSC of our pure nanostructured CeO$_2$ reduced at 673 K. This method does not hold for the SiO$_2$–CeO$_2$ composite material since silica skeletal vibrations hide spectral features below 1300 cm^{-1}. This difficulty was overcome by considering the ν(CH) vibration modes: the symmetrical elongation of the C–H bond is also sensitive to the oxidation state of the cerium cation,[31] with a shift in the frequency vibration from 2807 to 2782 cm^{-1} accompanying the Ce^{4+} → Ce^{3+} reduction reaction for the CeO$_2$ sample. Moreover, the apparition of an intense Fermi resonance (due to a shift of the δ(CH$_3$) vibration mode from 1447 to 1462 cm^{-1}) between the ν_a(CH$_3$) mode and the 2δ(CH$_3$) overtone generates two intense bands located at 2919 and 2836 cm^{-1}. On analysis of the evolution of the ν_a(CH$_3$) vibration band at 2921 cm^{-1} (for the composite material) or the shift of the ν_s(CH$_3$) stretch (Figure 6), an OSC value between 270 and 280 μmol g^{-1}, similar to that determined above, was recorded the pure CeO$_2$ nanostructured material. The method having therefore being validated, an OSC value of 170 μmol g^{-1} was obtained for the SiO$_2$–CeO$_2$ composite material using the same procedure, yielding a corresponding normalized value of 212 μmol g^{-1} of CeO$_2$. This value is slightly lower than the previous one determined for the pure CeO$_2$ nanostructured materials. Hence, the composite nanostructuration of the surface does not affect significantly the OSC of the CeO$_2$ nanodomains, a characteristic property of the CeO$_2$ material.

While maintaining an intrinsic property such as the oxygen storage capacity of CeO$_2$, we previously observed that the composite structure of the surface down to the nanoscale modifies some surface properties of the CeO$_2$ nanodomains. First, different values of the dispersive component of the surface energy were determined for the composite materials compared to the physical mixture of the pure materials. Second, the modification of surface energy by the nanostructure was corroborated by similar observations made during the chemisorption experiments. After chemisorption with a propionic acid probe, an outgassing temperature of 413 K was required for the pure CeO$_2$ nanostructured material. A reference SiO$_2$– CeO$_2$ sample, prepared from a physical mixture of pure nanostructured CeO$_2$ material and pure SiO$_2$ nanostruc-

Figure 7. CO_2 adsorption on a pure CeO_2 nanostructured material at room temperature (a) and then evacuation at 373 K (b) and 573 K (c).

tured material, required the same outgassing temperature of 413 K. In contrast, a lower outgassing temperature of 383 K was needed for the SiO_2-CeO_2 composite materials. These observations indicated some modification of the strength of the interactions between the propionic acid and the surfaces of CeO_2 domains partially embedded in the thin layers of silica.

Monitoring acid−base properties of pure CeO_2 surfaces represents a challenge for some catalytic applications such as the production of hydrogen involving the water gas shift reaction, i.e., $CO + H_2O \rightarrow H_2 + CO_2$. CeO_2 based material is reported as a good candidate for catalyzing[33] this reaction requiring oxygen storage capacity. To improve its long-term catalytic activity, industrial development of CeO_2 based materials for this application requires the minimization of the basic property of CeO_2 ensuring the inhibition of formation of carbonate species at the CeO_2 surfaces due to the presence of CO_2 formed from the water gas shift reaction. We will thus explore the acid−base properties of the CeO_2 arrays displaying high thermal stability and high surface area using FTIR spectroscopy.

Basic molecules, such as CO or pyridine, did not show modifications in the weak Lewis acid behavior of cerium oxide due to silica matrix embedding. CO_2 is a more appropriate probe since, after adsorption of CO_2 at room temperature, typical bands attributed to hydrogen−carbonates, monodentate, bidentate, and polydentate carbonates[29,30] were observed on our pure CeO_2 nanostructured material (Figure 7a). After evacuation at 373 K we observed the decomposition of hydrogen−carbonates (Figure 7b). Bidentate carbonates are stable until 573 K (Figure 7c). These observations are consistent with the basic character of CeO_2 surfaces usually reported in the literature.

Spectra recorded on SiO_2-CeO_2 composite materials (Figure 8) showed a completely different spectrum with hydrogen−carbonate bands (1594 and 1415 cm^{-1}), linearly adsorbed CO_2 (1377 cm^{-1}), and small amounts of monodentate carbonates (1510 cm^{-1}). These species are fully eliminated after evacuation at 373 K. Note that CO_2 adsorption on a pure mesostructured SiO_2 material indicates only physisorbed species developing low interactions with the OH of the silanol groups. We can therefore

(33) Fu, Q.; Weber, A.; Flytzani-Stephanopoulos, M. *Catal. Lett.* **2001**, 77, 1−3, 87.
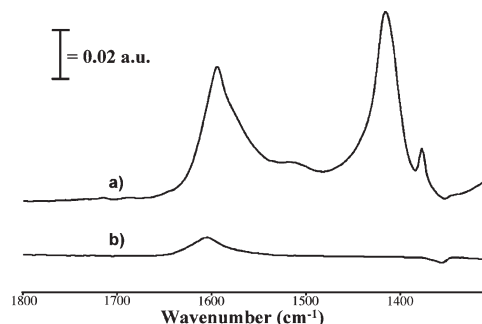
Figure 8. CO_2 adsorption on the $Si_{0.5}-Ce_{0.5}$ material at room temperature (a) and then evacuation at 373 K (b).

argue from these FTIR investigations that the CeO_2 nanodomains of the SiO_2-CeO_2 composite materials have displayed a lower basic character. The presence of hydrogen−carbonate species indicates the existence of OH basic sites in a higher proportion compared to oxygen basic sites, showing that the dispersion of CeO_2 nanodomains in the silica thin layer generates a high density of interfaces between silica and CeO_2 nanoparticles, resulting in a modification of the CeO_2 basic character. This illustrated that the composite nanostructuration approach can be exploited to tailor the acid−base properties of the CeO_2 surface for catalytic applications.

Conclusions

Ordered arrays of 5 nm CeO_2 nanoparticles, embedded in a thin layer of SiO_2, were investigated using SAXS, TEM, inverse chromatography, chemisorption, and FTIR techniques. A homogeneous distribution of the CeO_2 nanoparticles within ordered silica thin layers was found by TEM studies. From inverse chromatography at infinite dilution (IGC-ID), we showed that this preparation route produces materials displaying surface nanorugosity. Assessment of the accessibility to the CeO_2 surfaces through the porous volume was performed through an organic acid chemisorption study along a quantitative determination of the CeO_2 surface coverage ratio. From all these observations, we can conclude that the SiO_2-CeO_2 materials displayed a structured composite surface down to the nanometer scale produced by the emergence of 5 nm individualized CeO_2 nanoparticles from the SiO_2 thin layers. The ability to tune some of the surface properties such as its acid base character while preserving a fundamental property of CeO_2 such as the oxygen storage capacity, should offer new opportunities for these ordered arrays of CeO_2 nanoparticles. Preparation of a variety of nanoparticle arrays displaying high surface area and high thermal stability involving this approach will allow a wide range of applications to be explored such as catalysis, sensors, etc.